ACS OMEGA

http://pubs.acs.org/journal/acsodf

Article

Enhancing the Photoelectric Properties of Zinc Porphyrin Dyes by Introducing Five-Membered Heterocyclic Rings into the Electron Donor: A Density Functional Theory and Time-Dependent Density Functional Theory Study

Qingtang Yuan, Yanmin Yu,* Zhicheng Sun,* and Xufeng Song

Cite This: *ACS Omega* 2021, 6, 23551−23557

Read Online

ACCESS | Metrics & More | Article Recommendations | Supporting Information

ABSTRACT: To fabricate highly efficient dye sensitizers for dye-sensitized solar cells, new zinc porphyrin dye sensitizers were designed based on one of the most efficient dyes, YD2-*o*-C8, by introducing electron-rich heterocyclic rings into the electron donor. Five potentially efficient dyes, Dye1−5, were obtained by replacing the phenyl group of the donor in YD2-*o*-C8 with pyrrolyl, furyl, and thienyl groups. The electronic structures, absorption spectra, intramolecular charge-transfer characteristics, and excited-state lifetimes of the designed dyes were investigated using the density functional theory and time-dependent density functional theory methods. All the designed dyes exhibit better photoelectric properties than those of YD2-*o*-C8. Compared with YD2-*o*-C8, the designed new dyes have smaller frontier molecular orbital energy gaps and obvious red-shifting absorption spectra in the Q band. The analyses of charge density difference plots and intramolecular charge-transfer characteristics indicated that the designed dyes can better promote intramolecular charge transfer and electron−hole separation. Among the five designed dyes, Dye1 with a pyrrolyl group exhibits the best performance. Dye3 and Dye5 with methyl-furyl and methyl-thienyl groups, respectively, exhibit the next best performance. Dye2 and Dye4 with furyl and thienyl groups, respectively, are the worst performers. The introduced methyl group can further improve the electron-donating ability of heterocyclic rings and promote the red shift of the Q bands and intramolecular charge transfer of dyes. The excited-state lifetimes of the new dyes were in the following order: YD2-*o*-C8 < Dye4 < Dye2 < Dye5 < Dye3 < Dye1, which shows their stronger abilities to inject electrons into semiconductor films.

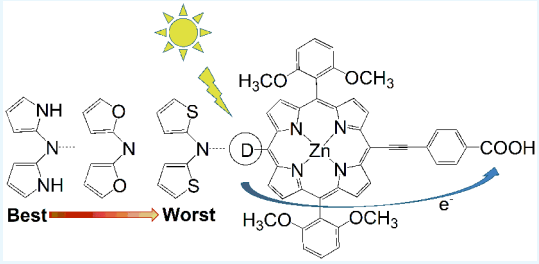

1. INTRODUCTION

With the gradual depletion of fossil fuels and continuous aggravation of the global greenhouse effect, the study of solar cells for cost-effective conversion of solar energy of a certain wavelength into electric power has attracted extensive attention.[1−5] In solar cell fields, a silicon-based solar cell occupies a major position due to the comparatively developed production technology and relatively high power conversion efficiency.[6,7] However, the production of silicon-based solar cells is accompanied by high energy consumption and environmental pollution. In order to solve these problems, scientists have carried out a lot of work on the third generation of solar cells including perovskite solar cells and dye-sensitized solar cells (DSSCs)[1−5,8] in which DSSCs have attracted significant attention because of their environment-friendliness, cost-effectiveness, and relatively high efficiencies.

The first DSSC was reported by Grätzel in 1991.[9] A typical sandwich-structure DSSC device consists of four main components: (I) a redox electrolyte; (II) a semiconductor film; (III) a counter electrode; and (IV) a dye sensitizer. Changing the electrolyte[10] and the semiconductor film[11,12] and modifying the structure of the dye[4] can promote the performance of DSSCs in which the structure of the dye sensitizer is a very important factor affecting the efficiency of DSSCs. The dye molecules as the core component of the DSSC system can absorb photons within a certain wavelength range and generate electrons. The wide-spectral solar energy would be effectively utilized and the performance of DSSCs can be improved by the controllable modification of the dye structure.[13] Among organic dyes, porphyrin derivatives are potential high-efficiency dye sensitizers because of their conjugated macrocyclic structures and multiple modifiable binding sites. Porphyrin dyes can hold different substitution groups to form an efficient structure for absorbing photons, releasing excitons, and realizing efficient photovoltaic con-

Received: July 9, 2021
Accepted: August 20, 2021
Published: September 2, 2021

https://doi.org/10.1021/acsomega.1c03635
ACS Omega 2021, 6, 23551−23557

version in DSSCs. In recent years, many zinc porphyrin dyes with high photovoltaic conversion performance have been studied.[14−16] Among them, bipolar D-π-A porphyrin dyes composed of an electron donor (D), a π-linker (π), and an electron acceptor (A) have received significant attention. In 2011, Grätzel synthesized a high-efficiency D-π-A zinc porphyrin dye, YD2-*o*-C8, with diphenylamine as the electron donor.[14] The cosensitization of YD2-*o*-C8 with Y123 achieved a higher photovoltaic conversion efficiency of 12.3%.[14] However, YD2-*o*-C8 suffers from the problem of narrower absorption in the near-infrared region. To overcome this problem, YD2-*o*-C8 was modified by changing its structure. Changing the structure of the π-linker in the dye can increase the conjugation degree of the dye and promote the effective localized separation of the highest occupied molecular orbital (HOMO) and the lowest unoccupied molecular orbital (LUMO), thus affecting the intramolecular charge transfer of the dye sensitizer and ultimately affecting the photoelectric conversion efficiency of the DSSCs.[17,18] Modifying the electron acceptor and anchoring groups in the dye can significantly affect the absorption of the dye onto the semiconductor film and the charge injection efficiency from the dye sensitizer to the semiconductor film,[19,20] while modifying the electron donor can narrow the frontier molecular orbital energy gap and promote the absorption of light energy in the long-wavelength region by appropriately increasing the HOMO energy level of the dye.[21,22] Based on YD2-*o*-C8, Grätzel synthesized the Y350-OC12 dye (Figure S1) by replacing the alkyl group of the electron donor with 2,4-dihexyloxyphenyl. Y350-OC12 showed a higher open-circuit photovoltage at both low light intensity and full sunlight intensity compared with YD2-*o*-C8.[23] The CM-b dye (Figure S2) with indoline as the electron donor was synthesized by You. The incident photon-to-current conversion efficiency values over nearly the whole spectrum for CM-b surpass those of the YD2-*o*-C8 cell under the same conditions. Moreover, the electron injection driving force from the LUMO of CM-b to the conduction band of TiO_2 is much higher than that of YD2-*o*-C8.[13] Xie et al. synthesized XW15 and XW16 (Figure S3), both of which used a triphenylamine moiety with various alkoxy chains as the electron donor to extend the spectrum absorption to a longer wavelength and improve the photovoltaic efficiency. Moreover, the incident photon-to-current conversion efficiency spectra of XW15 and XW16 exhibit a broader spectral response.[24] Ren et al. designed a potential high-efficiency dye, NCH_3-YD2 (Figure S4), by introducing $N(CH_3)_2$ groups at the diphenylamine electron donor of YD2-*o*-C8 and investigated it using density functional theory (DFT) and time-dependent density functional theory (TD-DFT). The results show that the introduced $N(CH_3)_2$ effectively improves the light harvesting efficiency and the intramolecular charge-transfer character compared with YD2-*o*-C8.[25] In addition, carbazol,[26] pyrenyl,[27] *N*-annulated perylene,[28] phenothiazinyl,[29,30] and some other heterocycles[31] can also be used as electron donors to obtain high-efficiency zinc porphyrin dyes.

A suitable electron donor must not only have an appropriate electron-donating ability to maintain a stable cycle between the dye and the redox electrolytes in DSSCs but also have a small frontier molecular orbital energy gap to reduce the photoexcitation energy and promote the absorption of light in the long-wavelength region. Pyrrolyl, furyl, and thienyl groups as electron-rich heterocycles have the potential to be used as electron donors in zinc porphyrin dyes. Although these heterocyclic groups have been studied as a π-linker,[32−35] there are hardly any studies on pyrrolyl, furyl, and thienyl groups as electron donors in zinc porphyrin dyes. In this study, a series of novel dyes was designed by introducing five-membered heterocyclic groups (pyrrolyl, furyl, and thienyl) as the electron donors using YD2-*o*-C8 as the basis. The structure of YD2-*o*-C8 is shown in Figure 1. To simplify computational

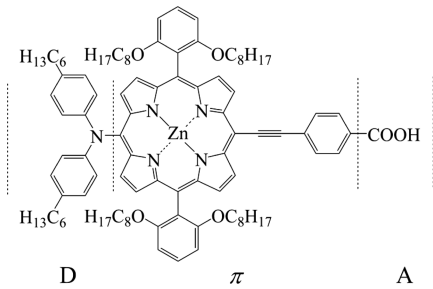

Figure 1. Structure of YD2-*o*-C8.

complexity, the alkyl and alkoxy groups of YD2-*o*-C8 were replaced by methyl and methoxy groups on the premise of keeping satisfactory accuracy.[36,37] The proposed D-π-A dye structures with various five-membered heterocyclic groups as electron donors are shown in Figure 2. In Dye1, the α-C atom

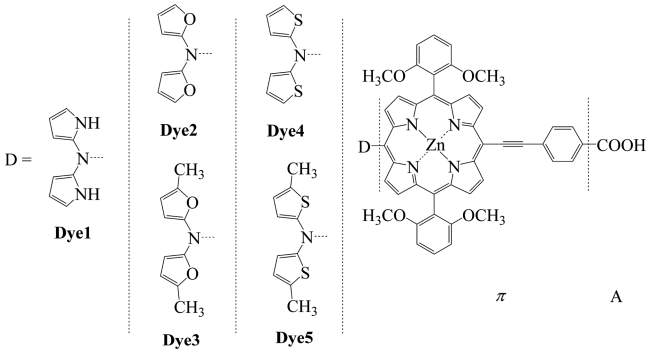

Figure 2. Structures of the designed dyes.

of pyrrolyl is connected to an amino N atom. In Dye2 and Dye3, the α-C atom of furyl and methyl-furyl is connected to the amino N atom, respectively. Dye4 and Dye5 have the α-C atom of the thienyl group connected to the amino N atom, respectively. The photoelectric properties of the proposed dyes were investigated using DFT and TD-DFT.

2. RESULTS AND DISCUSSION

2.1. Frontier Molecular Orbitals. The frontier molecular orbitals of a dye play an important role in determining the performance of DSSCs. However, the dye must have the HOMO energy level to maintain a stable cycle between the dye and redox electrolytes in DSSCs and the LUMO energy level to ensure efficient electron injection into the TiO_2 film and dye generation reactions. A narrower frontier molecular orbital energy gap (E_g) of the dye indicates a lower $\pi \rightarrow \pi^*$ transition energy, which can improve light-harvesting capacities and promote the red shifting of light absorption in the Q band. Frontier molecular orbital energy levels were calculated for the proposed dyes. The data for the HOMO, LUMO, and HOMO−LUMO gaps are shown in Figure 3. It is evident that the HOMO energy levels of Dye1−5 (from −5.10 to

https://doi.org/10.1021/acsomega.1c03635
ACS Omega 2021, 6, 23551−23557

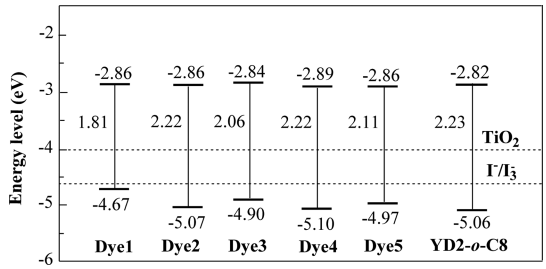

Figure 3. Computed HOMO and LUMO energy levels of dyes.

−4.67 eV) are lower than that of the redox potential of I^-/I_3^- (−4.6 eV),[38] indicating that the designed dyes are capable of obtaining electrons from I^-/I_3^- and can be efficiently reduced and regenerated. The LUMO energy levels of Dye1−5 (from −2.89 to −2.82 eV) are higher than the conduction band energy level of TiO_2 (−4.0 eV),[39] indicating that the designed dyes have enough driving force for electron transfer from the excited-state dye to the surface of the TiO_2 semiconductor. Compared with YD2-*o*-C8, introducing five-membered heterocyclic groups into the electron donor effectively increases the HOMO energy level of the dyes and leads to a decrease in the energy gap of the dyes. The narrower frontier molecular orbital energy gap may lead to lower $\pi \rightarrow \pi^*$ transition energy and red shift and the broadening of light absorption in the Q band of the dyes. Dye1 with the pyrrolyl group in the electron donor has the smallest frontier molecular orbital energy gap and is considered to be the most efficient dye. Furthermore, the methyl substituent in furyl and thienyl groups can decrease the frontier molecular orbital energy gap and increase the performance of the dye.

The distribution of frontier molecular orbitals is an important factor that significantly affects the intramolecular charge transfer of the dye and further affects the performance and efficiency of DSSCs. The ideal distribution of frontier molecular orbitals is that the HOMO is concentrated mainly in the electron donor part and the LUMO is concentrated mainly in the acceptor and π-linker of the dye, which is conducive to the realization of electron−hole separation and promotes intramolecular charge transfer. Figure 4 shows the distributions of the frontier molecular orbitals of the dyes. The distributions of LUMO are similar and concentrated in the π-linker. The HOMO distributions in Dye1−5 are more concentrated in the electron donor and less concentrated in the porphyrin ring

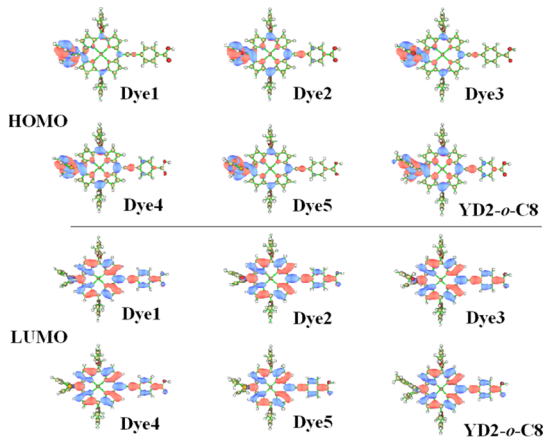

Figure 4. Frontier molecular orbitals of dyes.

compared with those in YD2-*o*-C8. This makes Dye1−5 to achieve better electron−hole separation and promote intramolecular charge transfer. To further explore the frontier molecular orbitals, the molecular orbital compositions of the dyes were analyzed. From Table 1, it can be seen that the

Table 1. Molecular Orbital Composition (%) of HOMO and LUMO of Dyes

dye	orbit	D	π	A
Dye1	HOMO	82.13	17.75	0.13
	LUMO	3.66	93.47	2.87
Dye2	HOMO	61.98	37.74	0.29
	LUMO	1.89	95.32	2.79
Dye3	HOMO	77.49	22.35	0.16
	LUMO	2.17	94.97	2.86
Dye4	HOMO	55.78	43.88	0.33
	LUMO	2.35	94.99	2.66
Dye5	HOMO	70.36	29.43	0.21
	LUMO	2.55	94.73	2.72
YD2-*o*-C8	HOMO	45.26	54.32	0.42
	LUMO	2.61	94.50	2.89

HOMOs of the dyes are gathered mainly in the electron donor, and the electron donor is the main occupier of the HOMO for the designed dyes. The order of the molecular orbital compositions of the HOMO in the donor for different dyes is YD2-*o*-C8 (45.26%) < Dye4 (55.78%) < Dye2 (61.98%) < Dye5 (70.36%) < Dye3 (77.49%) < Dye1 (82.13%). The donor of Dye1 occupies the largest molecular orbital composition of the HOMO. Dye1 has the best intramolecular charge-transfer ability. Moreover, the introduction of methyl groups in the heterocycles can enhance the properties of electron−hole separation.

2.2. Natural Transition Orbitals. The natural transition orbital (NTO)[40] can clarify the transition origins of electronic excitations. To further explore the characteristics of the $S_0 \rightarrow S_1$ orbital transition, NTO analysis was performed and the dominant NTO pairs involved in the S_1 excited states of dyes are shown in Figure 5. The values in Figure 5 represent the weight of the hole−electron wave function's contribution to the excitation. The enough large weight means that the NTO pair plays a leading role in the electron transition from $S_0 \rightarrow S_1$, and the characteristics of the orbital transition can be well represented by this one pair of transition orbital for the designed dyes and YD2-*o*-C8. By analyzing the hole state and the electron state of the NTO pair, it can be seen that for all of the dyes, the hole is mainly localized on the electron donor, while the electron shows delocalization on the π-linker and acceptor of dyes. The electron is moved from the donor to the π-linker and acceptor in the transition of dyes, which indicates the obvious intramolecular charge transfer of Dye1−5 and YD2-*o*-C8.

2.3. UV−vis Absorption Spectrum. The simulated absorption spectrum can reflect the absorption intensity and range of the dyes to photons. The broadened absorption spectrum increases the light-harvesting ability. The simulated absorption spectra are shown in Figure 6. They are similar to the porphyrin absorption spectra obtained by the experiment.[14] The characteristic absorption peaks in Soret bands are located at around 430 nm, and the absorption peaks of Q bands are located in the region of approximately 660−880 nm. The absorption peak in the Q band of YD2-*o*-C8 is located at

https://doi.org/10.1021/acsomega.1c03635
ACS Omega 2021, 6, 23551−23557

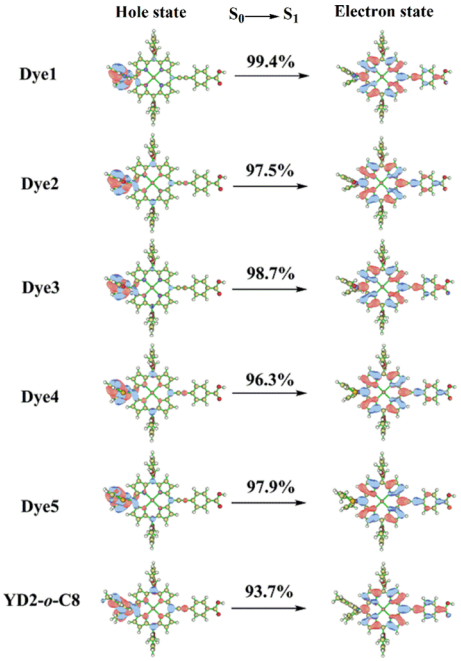

Figure 5. NTOs of the dyes. The weight of the hole−electron wave function's contribution to the excitations is also included.

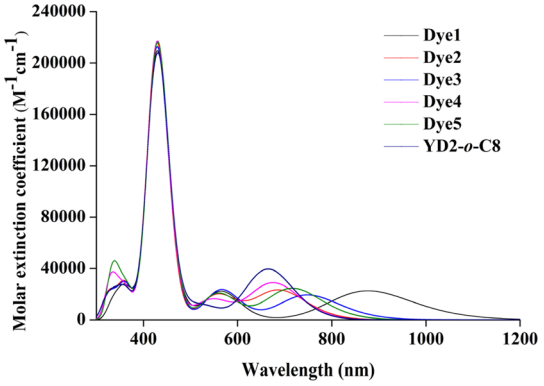

Figure 6. Simulated absorption spectra of dyes.

664 nm, whereas the absorption in the Q band region of Dye1−5 relative to YD2-*o*-C8 is red shifted and broadened significantly. The Q bands of Dye1−5 are located at 877, 686, 748, 675, and 716 nm, respectively. The degrees of the red shift of Dye1−5 relative to YD2-*o*-C8 follow the order Dye4 < Dye2 < Dye5 < Dye3 < Dye1 owing to the introduced electron-releasing five-membered heterocyclic groups. The tendencies of the red shift of the absorption in the Q band and the molecular orbital composition of the HOMO in the donor of the dyes are consistent. It is particularly worth noting that Dye1 shows the most obviously widest red shift and covers considerable visible and near-infrared regions, which is mainly attributed to the better electron-releasing ability of the pyrrolyl group of Dye1.

2.4. Intramolecular Charge Transfer. To evaluate the degree of electron−hole separation and quantitatively describe the intramolecular charge transfer properties of the dyes, the charge transfer distance (L), hole and electron separation degrees (t index),[41] and the vertical excitation energy (E_{exc}) were calculated using the TD-B3LYP method. These results are listed in Table 2. The larger values of L and the t index as well as the smaller values of E_{exc} are more favorable for intramolecular charge transfer. For the dyes, the calculated t index, E_{exc}, and L indicate the same tendency of performance of dyes: YD2-*o*-C8 < Dye4 < Dye2 < Dye5 < Dye3 < Dye1, which is consistent with the order of the molecular orbital compositions. The charge density difference plots (Figure 7)

Table 2. Charge Transfer Distance (L/Å), t Index (Å), and Vertical Excitation Energy (E_{exc}/eV) of Dyes

method	dye	L	t index	E_{exc}
B3LYP	Dye1	5.72	2.34	1.41
	Dye2	5.20	1.50	1.80
	Dye3	5.70	2.25	1.66
	Dye4	4.66	0.74	1.83
	Dye5	5.33	1.64	1.73
	YD2-*o*-C8	3.88	−0.25	1.87
CAM-B3LYP	Dye1	1.84	−1.96	1.94
	Dye2	0.32	−3.12	2.08
	Dye3	0.57	−2.98	2.06
	Dye4	0.36	−3.11	2.06
	Dye5	0.52	−3.02	2.05
	YD2-*o*-C8	0.42	−3.11	2.05

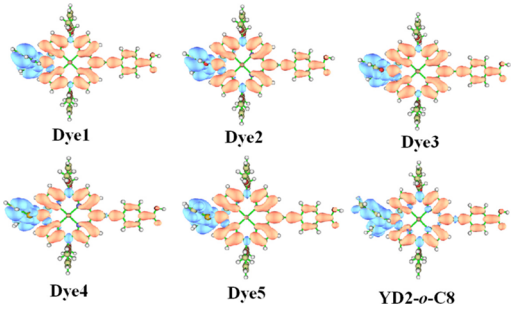

Figure 7. Charge density difference plots of dyes.

are shown to visualize the characteristics of the intramolecular charge transfer process. From Figure 7, it is evident that the dyes have zones with electron density depletion (blue) and increment (orange). Compared with YD2-*o*-C8, the blue parts of Dye1−5 are more concentrated in the donor and less concentrated in the porphyrin ring, while the orange part is more concentrated in the π-linker and electron acceptor. This indicates the better electron−hole separation for Dye1−5. In addition, the parameters describing the intramolecular charge transfer were also calculated using the TD-CAM-B3LYP method, and the results are listed in Table 2. The results from TD-CAM-B3LYP show a similar tendency of performance for the designed dyes with those of TD-B3LYP. Dye1 with pyrrolyl groups has the best ability to release electrons, which leads to Dye1 having the best ability to achieve intramolecular charge transfer and electron−hole separation. Dye2 and Dye4 with furyl and thienyl groups, respectively, have the weakest electron-donating ability of the donor and are the worst performers. Dye3 and Dye5 with methyl-furyl and methyl-thienyl groups, respectively, exhibit the next best performance due to the electron-releasing methyl groups.

2.5. Excited-State Lifetimes. The decay of the first excited state (S_1) to the ground state (S_0) is significant for the process of electron injection from the excited dye into the semiconductor film. A longer excited-state lifetime (τ) is conducive to the charge transfer from the dye to the

https://doi.org/10.1021/acsomega.1c03635
ACS Omega 2021, 6, 23551−23557

semiconductor film.[42,43] Therefore, τ of the excited-state dyes in the excited singlet electronic state becomes an important parameter for measuring the electron injection process, and τ robustly affects the transfer of electrons on zinc porphyrin dyes. The geometries of the molecules in the first excited singlet electronic state were optimized to investigate the lowest excitation energy and the related oscillator strength by TD-B3LYP combined with 6-31G(d) for the C, H, O, N, and S atoms and the LANL2DZ basis set for the Zn atom. Both the oscillator strength of the electronic state (f) and the lowest excitation energy of different electronic states (E) were calculated. The value of τ was calculated using the following formula: $\tau = 1.499/(fE^2)$.[38,44] The E (cm^{-1}) and f values are listed in Table S1. The τ values of the dyes are listed in Table 3. From Table 3, the improvement degree and the order of τ of the dyes are as follows: YD2-*o*-C8 < Dye4 < Dye2 < Dye5 < Dye3 < Dye1, which is consistent with the aforementioned orders. Therefore, it is believed that Dye1−5 with five-membered heterocyclic groups such as pyrrolyl, furyl, and thienyl groups perform better than YD2-*o*-C8 and have a stronger ability to inject electrons into the semiconductor film. Moreover, pyrrolyl groups have a more obvious influence on the performance of dyes compared to furyl and thienyl substituent groups. In particular, the improvement in τ of Dye1 can effectively inhibit the recombination of electrons and holes after excitation and then improve the power conversion efficiency of DSSCs. Furthermore, the electron-releasing methyl group in heterocyclic moieties can improve the τ of dyes.

Table 3. Calculated Excited-State Lifetime of Each Dye (ns)

dye	Dye1	Dye2	Dye3	Dye4	Dye5	YD2-*o*-C8
τ	2391.2	93.812	272.71	84.13	106.91	11.86

2.6. Ionization Potential, Electron Affinity, and Reorganization Energy. Ionization potential (IP) and electron affinity (EA) can be used to evaluate the efficiency of electron transport and injection of the dye. The lower IP reflects the higher electron-donating capability of the dye. The higher EA is favorable for electron injection. In addition, the intramolecular reorganization energy (Λ) can reveal the balance between the electron and hole transport, which includes the hole reorganization energy (Λ_h) and the electron reorganization energy (Λ_e). IP, EA, Λ_h, Λ_e, and Λ are calculated using the following formulas:[45]

$$EA = E_0 - E_0^-$$

$$IP = E_0^+ - E_0$$

$$\Lambda_h = (E_0^+ - E_+) + (E_+^0 - E_0)$$

$$\Lambda e = (E_0^- - E_-) + (E_-^0 - E_0)$$

$$\Lambda = \Lambda_h + \Lambda_e$$

E_0^+ and E_0^- are the energy of the cation and the anion based on the ground-state neutral dye, respectively. E_+ and E_- are the energy of the cation and the anion based on their lowest energy geometry, respectively. E_+^0 and E_-^0 are the energy of the neutral dye based on the optimized cation and anion states, respectively. E_0 is the energy of the optimized neutral dye. The corresponding calculation results of IP, EA, and Λ are listed in Table 4. With the introduction of five-membered heterocyclic groups in the dyes, the IP values decrease and the EA values increase. This indicates that the hole injection ability and the electron injection ability of dyes are improved. Moreover, the IP values decrease in the following order: Dye4 (5.09 eV) > Dye2 (5.07 eV) > Dye5 (4.97 eV) > Dye3 (4.92 eV) > Dye1 (4.71 eV). The minimum IP is observed in Dye1, which indicates that it is easier to release electrons and create holes in Dye1 than in other dyes. On the other hand, the smaller reorganization energy indicates a higher electron injection rate.

Table 4. Ionization Potential (IP/eV), Electron Affinity (EA/eV), and Internal Hole and Electron Reorganization Energies (Λ_h and Λ_e/eV) of Dyes

dye	IP	EA	Λ_h	Λ_e	Λ
Dye1	4.71	2.88	0.232	0.194	0.426
Dye2	5.07	2.87	0.196	0.148	0.344
Dye3	4.92	2.85	0.189	0.153	0.342
Dye4	5.09	2.90	0.190	0.156	0.346
Dye5	4.97	2.88	0.200	0.160	0.360
YD2-*o*-C8	5.03	2.84	0.205	0.150	0.355

3. CONCLUSIONS

Five novel porphyrin dye sensitizers with three different five-membered heterocyclic rings (furyl, pyrrolyl, and thienyl groups) for improved DSSCs were designed and studied using DFT and TD-DFT. Through a detailed comparison between Dye1−5 and YD2-*o*-C8, it was found that the proposed dyes not only have smaller HOMO−LUMO energy gaps and better abilities to transfer charges but also stronger spectral absorption characteristics, particularly a significant red shift of light absorption in the Q band. Furthermore, the proposed dyes have significantly longer excited-state lifetimes. Based on the results of the analyses, introducing suitable electron-donating groups such as five-membered heterocyclic groups can improve the energy conversion performance of dyes. We have strong reasons to believe that Dye1−5 with heterocyclic rings, particularly Dye1 with the pyrrolyl group, are potential candidates for high-efficiency DSSCs to improve their power conversion efficiency. It is expected that our theoretical research and design will be helpful for the experimental synthesis of efficient dyes for solar cells.

4. COMPUTATIONAL DETAILS

All the DFT and TD-DFT calculations were performed with Gaussian 16.[46] Both DFT and TD-DFT methods have been proved to be able to accurately evaluate the electronic and optical properties of organic dyes.[33,47−49] The initial geometry structures of the dyes are constructed based on the Zn porphyrin core. The charge is zero for all the dyes. The singlet ground-state geometries of the dyes were optimized using B3LYP[50] with the 6-311G(d, p) basis set for the C, H, O, N, and S atoms and the LANL2DZ basis set for the Zn atom. Frequency calculations were performed to ensure that the optimized singlet ground-state structures had no imaginary frequency. Based on the singlet ground-state-optimized structures, the TD-DFT calculations were carried out with the 6-31G(d) basis set for the C, H, O, N, and S atoms and the LANL2DZ basis set for the Zn atom to study the photoelectric properties of the singlet excited states of dyes. The solvent effect of the tetrahydrofuran medium was investigated using the polarized continuum model (PCM).[51] In the TD-DFT calculation, B3LYP,[50] CAM-B3LYP,[52] and ωB97X-D[53] were

https://doi.org/10.1021/acsomega.1c03635
ACS Omega 2021, 6, 23551−23557

benchmarked and used to calculate the absorption spectra of the reference dye YD2-*o*-C8, which has been studied experimentally.[14] The results are shown in Table S2. By comparison, the calculation results of B3LYP are closest to the experimental data. We also evaluated the calculation results of TD-B3LYP with different solvent models, as listed in Table S3. The results show that the PCM solvent model can better reproduce the experimental result of YD2-*o*-C8. Consequently, we chose the TD-B3LYP method with the PCM solvent model in our studies. UV−vis absorption spectra for the lowest 30 singlet excitations were recorded with a full width at half maximum of 0.33 eV. NTO, intramolecular charge-transfer characteristics, and charge density difference plots were analyzed with Multiwfn 3.8 package[54,55] to compare the abilities of charge transfer.

■ ASSOCIATED CONTENT

Supporting Information

The Supporting Information is available free of charge at https://pubs.acs.org/doi/10.1021/acsomega.1c03635.

Benchmark of various TD-DFT methods and solvent models against the experiment, the oscillator strength of the electronic state (f) and the lowest excitation energy of different electronic states (E/cm^{-1}) of the dyes, and the structures of dyes (PDF)

■ AUTHOR INFORMATION

Corresponding Authors

Yanmin Yu − *Beijing Key Laboratory for Green Catalysis and Separation, Department of Environmental Chemical Engineering, Beijing University of Technology, Beijing 100124, China;* orcid.org/0000-0002-4219-4611; Email: ymyu@bjut.edu.cn

Zhicheng Sun − *Beijing Engineering Research Center of Printed Electronics, School of Printing and Packaging Engineering, Beijing Institute of Graphic Communication, Beijing 102600, China;* orcid.org/0000-0003-3872-6782; Email: sunzhicheng@bigc.edu.cn

Authors

Qingtang Yuan − *Beijing Key Laboratory for Green Catalysis and Separation, Department of Environmental Chemical Engineering, Beijing University of Technology, Beijing 100124, China*

Xufeng Song − *Beijing Key Laboratory for Green Catalysis and Separation, Department of Environmental Chemical Engineering, Beijing University of Technology, Beijing 100124, China*

Complete contact information is available at: https://pubs.acs.org/10.1021/acsomega.1c03635

Notes

The authors declare no competing financial interest.

■ ACKNOWLEDGMENTS

This work was supported by the National Natural Science Foundation of China (No. 21376010 and 21776021), the Beijing Outstanding Young Scientists Program (BJJWZYJH0201910005017), the Beijing Municipal High-Level Innovative Team Building Program (IDHT20180504), and the Key Scientific Research Project of Beijing Municipal Commission of Education (KZ201910015016).

■ REFERENCES

(1) Jiao, S. Z.; Wen, J. Y.; Zhou, Y.; Sun, Z. C.; Liu, Y. Y.; Liu, R. P. Preparation and property studies of polyaniline film for flexible counter electrode of dye-sensitized solar cells by cyclic voltammetry. *ChemistrySelect* **2021**, *6*, 230−233.

(2) Jiao, S. Z.; Sun, Z. C.; Wen, J. Y.; Liu, Y. Y.; Li, F. R.; Miao, Q. Q.; Wu, W. X.; Li, L. H.; Zhou, Y. Development of rapid curing SiO_2 aerogel composite-based quasi-solid-state dye-sensitized solar cells through screen-printing technology. *ACS Appl. Mater. Interfaces* **2020**, *12*, 48794−48803.

(3) Choi, H.; Chen, W. T.; Kamat, P. V. Know thy nano neighbor. Plasmonic versus electron charging effects of metal nanoparticles in dye-sensitized solar cells. *ACS Nano* **2012**, *6*, 4418−4427.

(4) Zeng, K. W.; Tong, Z. F.; Ma, L.; Zhu, W. H.; Wu, W. J.; Xie, Y. S. Molecular engineering strategies for fabricating efficient porphyrin-based dye-sensitized solar cells. *Energy Environ. Sci.* **2020**, *13*, 1617−1657.

(5) Feng, X. X.; Lv, X. D.; Liang, Q.; Cao, J.; Tang, Y. Diammonium porphyrin-induced $CsPbBr_3$ nanocrystals to stabilize perovskite films for efficient and stable solar cells. *ACS Appl. Mater. Interfaces* **2020**, *12*, 16236−16242.

(6) Yoshikawa, K.; Kawasaki, H.; Yoshida, W.; Irie, T.; Konishi, K.; Nakano, K.; Uto, T.; Adachi, D.; Kanematsu, M.; Uzu, H.; Yamamoto, K. Silicon heterojunction solar cell with interdigitated back contacts for a photoconversion efficiency over 26%. *Nat. Energy* **2017**, *2*, 17032.

(7) Green, M. A.; Hishikawa, Y.; Dunlop, E. D.; Levi, D. H.; Hohl-Ebinger, J.; Ho-Baillie, A. W. Y. Solar cell efficiency tables (version 52). *Prog. Photovolt.* **2018**, *26*, 427−436.

(8) Chi, W. J.; Li, Q. S.; Li, Z. S. Exploring the electrochemical properties of hole transport materials with spiro-cores for efficient perovskite solar cells from first-principles. *Nanoscale* **2016**, *8*, 6146−6154.

(9) O'Regan, B.; Grätzel, M. A low-cost, high-efficiency solar cell based on dye-sensitized colloidal TiO2 films. *Nature* **1991**, *353*, 737−740.

(10) Grätzel, M. Photoelectrochemical cells. *Nature* **2001**, *414*, 338−344.

(11) Motlak, M.; Hamza, A. M.; Hammed, M. G.; Barakat, N. A. M. Cd-doped TiO_2 nanofibers as effective working electrode for the dye sensitized solar cells. *Mater. Lett.* **2019**, *246*, 206−209.

(12) Wang, X. F.; Li, Y. Z.; Song, P.; Ma, F. C.; Yang, Y. H. Effect of graphene between photoanode and sensitizer on the intramolecular and intermolecular electron transfer process. *Phys. Chem. Chem. Phys.* **2020**, *22*, 6391−6400.

(13) Li, C. M.; Luo, L.; Wu, D.; Jiang, R. Y.; Lan, J. B.; Wang, R. L.; Huang, L. Y.; Yang, S. Y.; You, J. S. Porphyrins with intense absorptivity: Highly efficient sensitizers with a photovoltaic efficiency of up to 10.7% without a cosensitizer and a coabsorbate. *J. Mater. Chem. A* **2016**, *4*, 11829−11834.

(14) Yella, A.; Lee, H. W.; Tsao, H. N.; Yi, C. Y.; Chandiran, A. K.; Nazeeruddin, M. K.; Diau, E. W. G.; Yeh, C. Y.; Zakeeruddin, S. M.; Grätzel, M. Porphyrin-sensitized solar cells with cobalt (II/III)-based redox electrolyte exceed 12 percent efficiency. *Science* **2011**, *334*, 629−634.

(15) Yella, A.; Mai, C. L.; Zakeeruddin, S. M.; Chang, S. N.; Hsieh, C. H.; Yeh, C. Y.; Grätzel, M. Molecular engineering of push-pull porphyrin dyes for highly efficient dye-sensitized solar cells: The role of benzene spacers. *Angew. Chem., Int. Ed.* **2014**, *126*, 3017−3021.

(16) Mathew, S.; Yella, A.; Gao, P.; Humphry-Baker, R.; Curchod, B. F. E.; Ashari-Astani, N.; Tavernelli, I.; Rothlisberger, U.; Nazeeruddin, M. K.; Grätzel, M. Dye-sensitized solar cells with 13% efficiency achieved through the molecular engineering of porphyrin sensitizers. *Nat. Chem.* **2014**, *6*, 242−247.

(17) Haid, S.; Marszalek, M.; Mishra, A.; Wielopolski, M.; Teuscher, J.; Moser, J. E.; Humphry-Baker, R.; Zakeeruddin, S. M.; Grätzel, M.; Bäuerle, P. Significant improvement of dye-sensitized solar cell performance by small structural modification in π-conjugated donor-acceptor dyes. *Adv. Funct. Mater.* **2012**, *22*, 1291−1302.

(18) Qian, X.; Lu, L.; Zhu, Y. Z.; Gao, H. H.; Zheng, J. Y. Phenothiazine-functionalized push-pull Zn porphyrin photosensitizers for efficient dye-sensitized solar cells. *RSC Adv.* **2016**, *6*, 9057−9065.
(19) Zhang, L.; Cole, J. M. Anchoring groups for dye-sensitized solar cells. *ACS Appl. Mater. Interfaces* **2015**, *7*, 3427−3455.
(20) Higashino, T.; Nimura, S.; Sugiura, K.; Kurumisawa, Y.; Tsuji, Y.; Imahori, H. Photovoltaic properties and long-term durability of porphyrin-sensitized solar cells with silicon-based anchoring groups. *ACS Omega* **2017**, *2*, 6958−6967.
(21) Xie, Y. S.; Tang, Y. Y.; Wu, W. J.; Wang, Y. Q.; Liu, J. C.; Li, X.; Tian, H.; Zhu, W. H. Porphyrin cosensitization for a photovoltaic efficiency of 11.5%: A record for non-ruthenium solar cells based on iodine electrolyte. *J. Am. Chem. Soc.* **2015**, *137*, 14055−14058.
(22) Chou, H. H.; Reddy, K. S. K.; Wu, H. P.; Guo, B. C.; Lee, H. W.; Diau, E. W. G.; Hsu, C. P.; Yeh, C. Y. Influence of phenylethynylene of push-pull zinc porphyrins on the photovoltaic performance. *ACS Appl. Mater. Interfaces* **2016**, *8*, 3418−3427.
(23) Yi, C. Y.; Giordano, F.; Cevey-Ha, N. L.; Tsao, H. N.; Zakeeruddin, S. M.; Grätzel, M. Influence of structural variations in push-pull zinc porphyrins on photovoltaic performance of dye-sensitized solar cells. *ChemSusChem* **2014**, *7*, 1107−1113.
(24) Tang, Y. Y.; Wang, Y. Q.; Li, X.; Ågren, H.; Zhu, W. H.; Xie, Y. S. Porphyrins containing a triphenylamine donor and up to eight alkoxy chains for dye-sensitized solar cells: A high efficiency of 10.9%. *ACS Appl. Mater. Interfaces* **2015**, *7*, 27976−27985.
(25) Kang, G. J.; Song, C.; Ren, X. F. Charge transfer enhancement in the D-π-A type porphyrin dyes: A density functional theory (DFT) and time-dependent density functional theory (TD-DFT) study. *Molecules* **2016**, *21*, 1618.
(26) Wang, Y. Q.; Chen, B.; Wu, W. J.; Li, X.; Zhu, W. H.; Tian, H.; Xie, Y. S. Efficient solar cells sensitized by porphyrins with an extended conjugation framework and a carbazole donor: From molecular design to cosensitization. *Angew. Chem., Int. Ed.* **2014**, *53*, 10779−10783.
(27) Lu, J. F.; Liu, S. S.; Li, H.; Shen, Y.; Xu, J.; Cheng, Y. B.; Wang, M. K. Pyrene-conjugated porphyrins for efficient mesoscopic solar cells: The role of the spacer. *J. Mater. Chem. A* **2014**, *2*, 17495−17501.
(28) Luo, J.; Zhang, J.; Huang, K. W.; Qi, Q. B.; Dong, S. Q.; Zhang, J.; Wang, P.; Wu, J. S. N-Annulated perylene substituted zinc-porphyrins with different linking modes and electron acceptors for dye sensitized solar cells. *J. Mater. Chem. A* **2016**, *4*, 8428−8434.
(29) Lu, Y. Y.; Cheng, Y. C.; Li, C. J.; Luo, J. X.; Tang, W. Q.; Zhao, S. L.; Liu, Q. Y.; Xie, Y. S. Efficient solar cells based on cosensitizing porphyrin dyes containing a wrapped donor, a wrapped π-framework and a substituted benzothiadiazole unit. *Sci. China: Chem.* **2019**, *62*, 994−1000.
(30) Song, H. L.; Li, X.; Ågren, H.; Xie, Y. S. Branched and linear alkoxy chains-wrapped push-pull porphyrins for developing efficient dye-sensitized solar cells. *Dyes Pigm.* **2017**, *137*, 421−429.
(31) Mathew, S.; Astani, N. A.; Curchod, B. F. E.; Delcamp, J. H.; Marszalek, M.; Frey, J.; Rothlisberger, U.; Nazeeruddin, M.K.; Grätzel, M. Synthesis, characterization and ab initio investigation of a panchromatic ullazine−porphyrin photosensitizer for dye-sensitized solar cells. *J. Mater. Chem. A* **2016**, *4*, 2332−2339.
(32) Liu, H. Z.; Li, B. Q.; Xue, B. C.; Liu, E. B. Theoretical design of high-performance boron dipyrromethenes dyes by introducing heterocyclics to tune photoelectric properties. *J. Phys. Chem. C* **2019**, *123*, 26047−26056.
(33) Kita, H.; Yamakado, R.; Fukuuchi, R.; Konishi, T.; Kamada, K.; Haketa, Y.; Maeda, H. Switching of two-photon optical properties by anion binding of pyrrole-based boron diketonates through conformation change. *Chem. − Eur. J.* **2020**, *26*, 3404−3410.
(34) Hu, W. X.; Yu, P.; Zhang, Z. M.; Shen, W.; Li, M.; He, R. X. Theoretical study of YD2-*o*-C8-based derivatives as promising sensitizers for dye-sensitized solar cells. *J. Mater. Sci.* **2017**, *52*, 1235−1245.
(35) Lee, G. H.; Kim, Y. S. Theoretical study of novel porphyrin-based dye for efficient dye-sensitized solar cell. *Mol. Cryst. Liq. Cryst.* **2017**, *645*, 168−174.
(36) Liu, D. S.; Ding, W. L.; Zhu, K. L.; Geng, Z. Y.; Wang, D. M.; Zhao, X. L. The master factors influencing the efficiency of D-A-π-A configurated organic sensitizers in dye-sensitized solar cell via theoretically characterization: Design and verification. *Dyes Pigm.* **2014**, *105*, 192−201.
(37) Ding, W. L.; Wang, D. M.; Geng, Z. Y.; Zhao, X. L.; Xu, W. B. Density functional theory characterization and verification of high−performance indoline dyes with D-A-π-A architecture for dye-sensitized solar cells. *Dyes Pigm.* **2013**, *98*, 125−135.
(38) Zhang, G. L.; Bai, Y.; Li, R. Z.; Shi, D.; Wenger, S.; Zakeeruddin, S. M.; Grätzel, M.; Wang, P. Employ a bisthienothiophene linker to construct an organic chromophore for efficient and stable dye-sensitized solar cells. *Energy Environ. Sci.* **2009**, *2*, 92−95.
(39) Asbury, J. B.; Wang, Y. Q.; Hao, E. C.; Ghosh, H. N.; Lian, T. Q. Evidences of hot excited state electron injection from sensitizer molecules to TiO_2 nanocrystalline thin films. *Res. Chem. Intermed.* **2001**, *27*, 393−406.
(40) Martin, R. L. Natural transition orbitals. *J. Chem. Phys.* **2003**, *118*, 4775−4777.
(41) Le Bahers, T.; Adamo, C.; Ciofini, I. A qualitative index of spatial extent in charge-transfer excitations. *J. Chem. Theory Comput.* **2011**, *7*, 2498−2506.
(42) Chen, S. L.; Yang, L. N.; Li, Z. S. How to design more efficient organic dyes for dye-sensitized solar cells? Adding more sp2-hybridized nitrogen in the triphenylamine donor. *J. Power Sources* **2013**, *223*, 86−93.
(43) Yang, L. N.; Sun, Z. Z.; Chen, S. L.; Li, Z. S. The effects of various anchoring groups on optical and electronic properties of dyes in dye-sensitized solar cells. *Dyes Pigm.* **2013**, *99*, 29−35.
(44) Chaitanya, K.; Ju, X. H.; Heron, B. M. Theoretical study on the light harvesting efficiency of zinc porphyrin sensitizers for DSSCs. *RSC Adv.* **2014**, *4*, 26621−26634.
(45) Datta, A.; Mohakud, S.; Pati, S. K. Comparing the electron and hole mobilities in the α and β phases of perylene: role of π-stacking. *J. Mater. Chem.* **2007**, *17*, 1933−1938.
(46) Frisch, M. J.; Trucks, G. W.; Schlegel, H. B.; Scuseria, G. E.; Robb, M. A.; Cheeseman, J. R.; Scalmani, G.; Barone, V.; Petersson, G. A.; et al. *Gaussian 16*; Gaussian, Inc.: Wallingford, CT, 2016.
(47) Santhanamoorthi, N.; Lo, C. M.; Jiang, J. C. Molecular design of porphyrins for dye-sensitized solar cells: A DFT/TDDFT study. *J. Phys. Chem. Lett.* **2013**, *4*, 524−530.
(48) Karthikeyan, S.; Lee, J. Y. Zinc-porphyrin based dyes for dye-sensitized solar cells. *J. Phys. Chem. A* **2013**, *117*, 10973−10979.
(49) Jin, X. Y.; Li, D. Y.; Sun, L. B.; Wang, C. L.; Bai, F. Q. Theoretical design of porphyrin sensitizers with different acceptors for application in dye-sensitized solar cells. *RSC Adv.* **2018**, *8*, 19804−19810.
(50) Becke, A. D. Density-functional thermochemistry. III. The role of exact exchange. *J Chem. Phys.* **1993**, *98*, 5648−5652.
(51) Tomasi, J.; Mennucci, B.; Cammi, R. Quantum mechanical continuum solvation models. *Chem. Rev.* **2005**, *105*, 2999−3094.
(52) Yanai, T.; Tew, D. P.; Handy, N. C. A new hybrid exchange-correlation functional using the coulomb-attenuating method (CAM-B3LYP). *Chem. Phys. Lett.* **2004**, *393*, 51−57.
(53) Chai, J. D.; Head-Gordon, M. Long-range corrected hybrid density functionals with damped atom-atom dispersion corrections. *Phys. Chem. Chem. Phys.* **2008**, *10*, 6615−6620.
(54) Lu, T.; Chen, F. Multiwfn: A multifunctional wavefunction analyzer. *J. Comput. Chem.* **2012**, *33*, 580−592.
(55) Liu, Z. Y.; Lu, T.; Chen, Q. X. An sp-hybridized all-carboatomic ring, cyclo[18]carbon: Electronic structure, electronic spectrum, and optical nonlinearity. *Carbon* **2020**, *165*, 461−467.

https://doi.org/10.1021/acsomega.1c03635
ACS Omega 2021, 6, 23551−23557